Selective Removal of Metallic Single-Walled Carbon Nanotubes with Small Diameters by Using Nitric and Sulfuric Acids

Cheol-Min Yang,[†] Jin Sung Park,[†] Kay Hyeok An,[†] Seong Chu Lim,[†] Kwanyong Seo,[‡] Bongsoo Kim,[‡] Kyung Ah Park,[†] Seungwu Han,[§] Chong Yun Park,[†] and Young Hee Lee*,[†]

BK21 Physics Division, Institute of Basic Science, Center for Nanotubes and Nanostructured Composites, Sungkyunkwan University, Suwon 440-746, Republic of Korea, Department of Chemistry, Korea Advanced Institute of Science & Technology, 373-1, Guseong-dong, Yuseong-gu, Daejeon 305-701, Republic of Korea, and Department of Physics, Division of Nano Science, Ewha Womans University, Seoul 120-750, Republic of Korea

Received: June 16, 2005; In Final Form: August 23, 2005

Coexistence of metallic and semiconducting carbon nanotubes has often been a bottleneck in many applications and much fundamental research. Single-walled carbon nanotubes (SWCNTs) were dissolved in HNO_3/H_2SO_4 mixture to confirm differing reactivity between metallic (m) and semiconducting (s) SWCNTs. With HNO_3/H_2SO_4 treatment, s-SWCNTs remained intact, while m-SWCNTs were completely removed for SWCNTs with small diameters less than 1.1 nm, which was confirmed by resonant Raman and optical absorption spectra. We also showed that nitronium ions (NO_2^+) dissolved in the HNO_3/H_2SO_4 solution could preferably attack the m-SWCNTs, which was supported by our theoretical calculation. This clear selectivity can be explained by the preferential adsorption of positively charged NO_2^+ on m-SWCNTs due to more available electron densities at the Fermi level in the m-SWCNTs. We report for the first time a selective removal of small-diameter m-SWCNTs by using HNO_3/H_2SO_4 solution, which presented a striking contrast to the diameter-selective removal of SWCNTs by oxidative etching reported previously.

Introduction

The electronic structures of carbon nanotubes are determined by their chirality and diameter. Coexistence of metallic and semiconducting carbon nanotubes in the conventionally synthesized samples has been a serious obstacle in many applications and much fundamental research. Despite tremendous demand for the use of carbon nanotubes with a specific chirality in large-scale application to various devices, for instance, nanotransistors and memory devices that necessitate semiconducting nanotubes,[1] and electrodes for batteries and supercapacitors that favor the metallic ones,[2] a chirality control has not been realized in the conventional synthesis approaches.[3−5] Although several selective separation methods have been reported by posttreatment such as dielectrophoresis, surfactant, DNA, bromination, diazonium, and solution-phase oxmylation,[6−12] a realistic separation method for high yield and massive quantities with a specific chirality of nanotubes is still highly desired. Furthermore, the fundamental reaction mechanism of nanotubes with adsorbates is still far from being clearly understood. In addition, according to previous reports, single-walled carbon nanotubes (SWCNTs) showed an oxidative etching effect, particularly small-diameter nanotubes.[13,14] Recently, Banerjee and Wong demonstrated diameter-selective reaction of SWCNTs toward ozonation.[15] Yudasaka et al. also reported the diameter-selective removal of SWCNTs by using light-assisted oxidation.[16] However, these studies did not provide any evidence for selective reactivity dependent on metallicity of SWCNTs. Although Menna et al. investigated selectivity in a chemically oxidative attack of SWCNTs in a mixed solution of nitric and sulfuric acids (HNO_3 and H_2SO_4), they did not report on the metallicity-dependent selective reactivity particularly in small-diameter nanotubes and merely concluded that the nanotube diameter is the most important factor in determining their reactivity and destruction.[17] In our previous study, we reported the effect of nitronium ion (NO_2^+) in the selective removal of small-diameter metallic (m) SWCNTs.[18] We treated the HiPco SWCNTs with nitronium hexafluoroantimonate (NO_2SbF_6; NHFA), which can produce NO_2^+. According to the Raman spectra of the NHFA-treated HiPco SWCNTs, the semiconducting (s) SWCNTs remained intact with the NHFA treatment, while the m-SWCNTs were removed at small diameters less than 1.1 nm.[18]

Here, we report for the first time a selective removal of m-SWCNTs with small diameters by using HNO_3/H_2SO_4 solution, which could be achieved by adjusting the treatment conditions. We dissolved the SWCNT powder in a mixed solution of HNO_3 and H_2SO_4 to determine differing reactivity between m-SWCNTs and s-SWCNTs in the solution. After HNO_3/H_2SO_4 treatment, s-SWCNTs remained intact, while m-SWCNTs were completely destroyed and removed, especially nanotubes with diameters in a range of 0.9−1.1 nm, which was confirmed by resonant Raman spectra and optical absorption spectra. This result can be explained by the charge transfer from m-SWCNTs to NO_2^+ dissolved in the HNO_3/H_2SO_4 solution, in good agreement with our theoretical calculations.

* To whom correspondence should be addressed. Fax: +82-31-290-5954. E-mail: leeyoung@skku.edu.
[†] Sungkyunkwan University.
[‡] Korea Advanced Institute of Science & Technology.
[§] Ewha Womans University.

10.1021/jp053245c CCC: $30.25
Published on Web 09/24/2005

Experimental Section

The 50 mg batches of pristine HiPco SWCNTs (Carbon Nanotechnologies Inc., two different batches) were immersed without pretreatment and stirred at room temperature in 50 mL mixtures of HNO_3 (60%)/H_2SO_4 (97%) with three different volume ratios (1:9, 1:3, and 1:2) for 12 and 48 h, respectively. This solution was filtrated through a membrane filter with a pore diameter of 10 μm and then washed with distilled water several times. After the leftover nanotubes on the filter and filtrated ones were dried, these samples were further heat-treated in Ar atmosphere for 1 h at 900 °C.

Field-emission scanning electron microscopy (FESEM) observations were carried out using a JSM6700F (JEOL) at 15 kV accelerating voltage. Raman spectroscopy measurements were performed using a microprobe RM1000 (Renishaw) at room temperature under ambient conditions. The Raman spectra were obtained by using excitation lasers with several wavelengths of 514 (Ar ion laser), 633 (He−Ne laser), and 785 nm (diode laser). To obtain optical absorption spectra (JASCO V-570), the powder sample was dissolved in 2-propanol and sprayed on the quartz substrate followed by heat treatment at 900 °C in Ar atmosphere. X-ray photoelectron spectroscopy (XPS; ESCA2000) was also taken to investigate the adsorbate effects. The measurements were done with Mg Kα excitation in a vacuum ($<10^{-6}$ Pa) at room temperature. Theoretical calculations were performed within a generalized gradient approximation (GGA)[19] using the computational package of PWSCF.[20] We employed ultrasoft pseudopotential for ionic potentials,[21] and the Kohn−Sham wave functions were described by plane waves with an energy cutoff of 35 Ry. The total charge of the system was maintained at zero due to the difficulties of modeling a charged system within the plane wave method. We defined an adsorption energy of molecules as $E_{ad} = E_{tot}$(adsorbate+CNT) $- E_{tot}$(adsorbate) $- E_{tot}$(CNT), where E_{tot} is the total energy of a given system. The atomic positions were fully relaxed until the forces on each atom became less than 0.001 atomic unit.

Results and Discussion

Strong acid treatments of nanotubes have been introduced traditionally for purification, chemical oxidation, modification of lengths, and functionalization of the nanotube ends.[22−25] Here we used various volume ratios of HNO_3/H_2SO_4 (1:9, 1:3, and 1:2) to investigate a selective attack of m-SWCNTs. In our approach, the HNO_3/H_2SO_4 treatment conditions (lower reaction temperature and no sonication) were rather mild, compared to the typical HNO_3/H_2SO_4 treatment for severe nanotube modification.[17,23,24] It is well-known that mixing HNO_3 and H_2SO_4 yields a high production rate of NO_2^+ as follows, which can easily attack π electrons in aromatic rings, leading to nitration.[26]

$$HNO_3 + 2H_2SO_4 \leftrightarrow NO_2^+ + H_3O^+ + 2HSO_4^-$$

The concentration of NO_2^+ produced from HNO_3/H_2SO_4 solution, which is directly dependent on the volume ratio of HNO_3 and H_2SO_4, increases in the following order: HNO_3/H_2SO_4 (1:9) < HNO_3/H_2SO_4 (1:2) < HNO_3/H_2SO_4 (1:3).

By analogy, we conjecture that NO_2^+ can attack π electrons on the carbon nanotube surface, which may lead to strong adsorption of NO_2^+ on the nanotube surface and subsequent modification or disintegration of the nanotube wall by an oxidative etching. The most intriguing idea is that the m-SWCNTs can provoke stronger adsorption of NO_2^+ with higher binding energy than s-SWCNTs due to more available charge density at the Fermi level which induces stronger charge transfer from SWCNT to NO_2^+, similar to the diazonium adsorbates.[11]

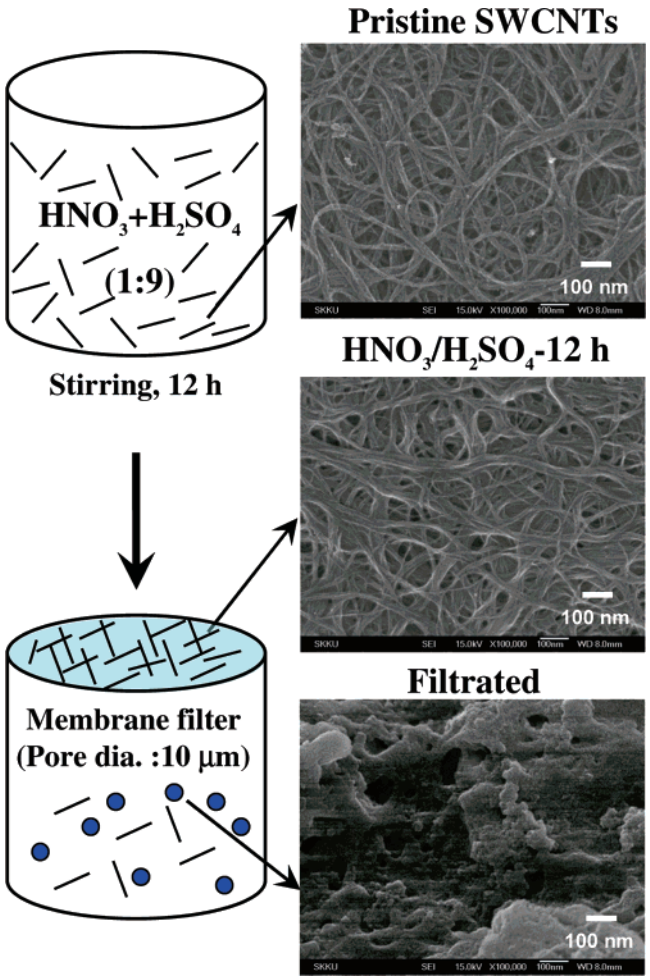

Figure 1. Schematic representation of HNO_3/H_2SO_4 treatment for HiPco SWCNTs and corresponding FESEM images of the pristine, the leftover on the filter, and the filtrated samples after HNO_3/H_2SO_4 (1:9) treatment for 12 h.

After the filtration followed by the HNO_3/H_2SO_4 (1:9) treatment, the morphology of the leftover nanotubes on the filter was similar to that of the pristine sample. However, the bundle size was slightly enlarged due to an aggregation effect in the solution (Figure 1). On the other hand, the filtrated SWCNTs in the precipitates were cut into small pieces and mostly disintegrated to carbonaceous particles, as shown in Figure 1. The leftover on the filter amounted to 65−70 wt %, depending on batches of HiPco SWCNTs used in the present study.

The selectivity in the metallicity with HNO_3/H_2SO_4 treatment can be clearly demonstrated in the resonant Raman spectra. All the samples were heat-treated in Ar gas ambient at 900 °C after the HNO_3/H_2SO_4 treatment. We identified various characteristic peaks in the radial breathing mode (RBM) using excitation lasers with three wavelengths (514, 633, and 785 nm). The diameters of SWCNTs were determined by the relation of ω (cm^{-1}) = 233/d (nm) + 14.[27] At 514 nm, we clearly observed two groups of s-SWCNTs near 183 cm^{-1} and m-SWCNTs near 260 cm^{-1} in the RBM of the pristine sample (Figure 2a) (characteristics of m- and s-SWCNTs were determined from the Kataura plot that is expressed by the relationship between transition energies and nanotube diameter[28]). The metallic peaks (m-peaks) near 260 cm^{-1} (diameter ~ 0.95 nm) disappeared completely after HNO_3/H_2SO_4 (1:9) treatments for 12 and 48 h and subsequent heat treatment in Ar gas ambient. On the other hand, the

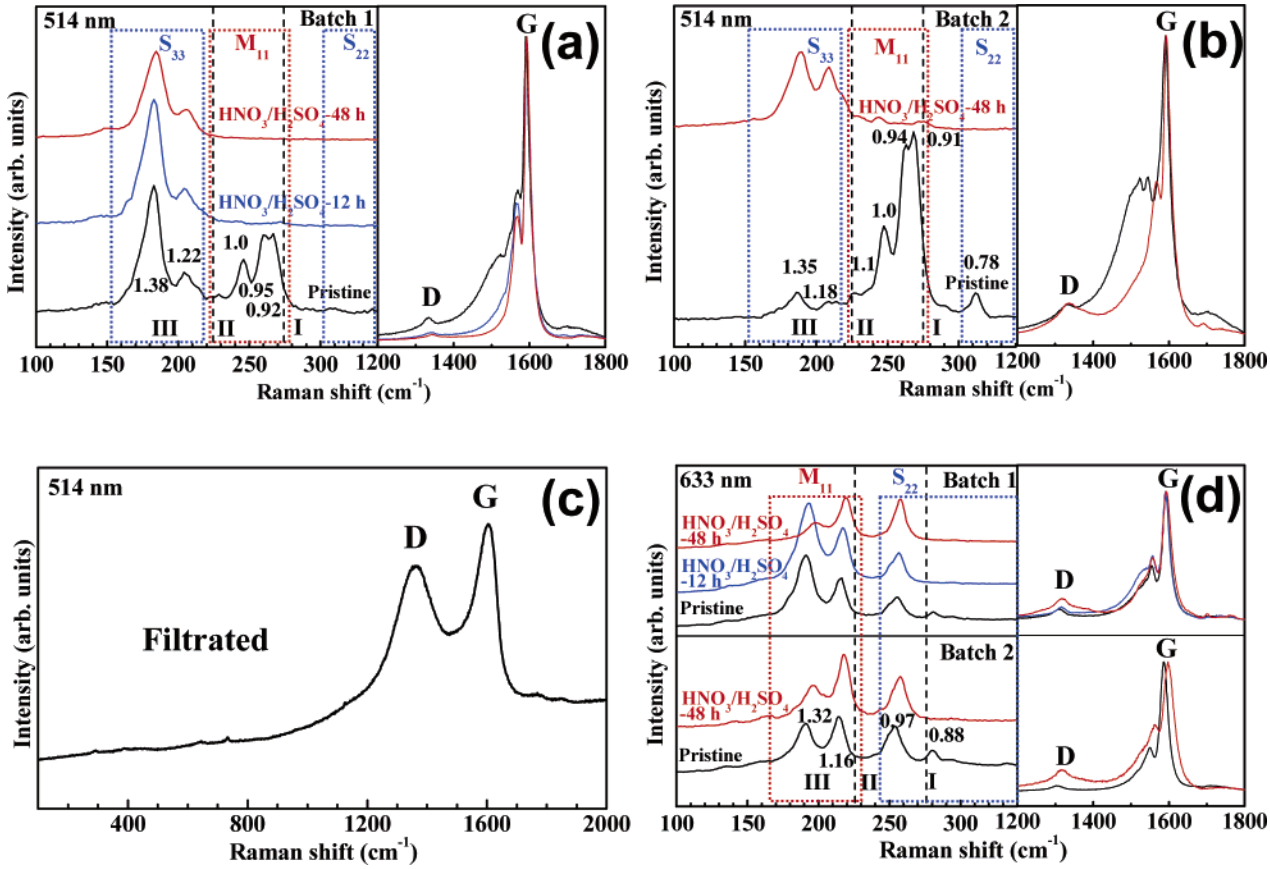

Figure 2. Raman spectra for HiPco SWCNTs. (a, b) RBM and G-band Raman spectra from the leftover on the filter for batch 1 and 2 HiPco SWCNTs at 514 nm excitation wavelength. The bottom (black), middle (blue), and top (red) lines are from the pristine, HNO_3/H_2SO_4 (1:9) treatment for 12 h, and HNO_3/H_2SO_4 (1:9) treatment for 48 h, respectively, followed by heat treatment at 900 °C in Ar atmosphere. (c) Raman spectrum of the filtrated sample after HNO_3/H_2SO_4 (1:9) treatment for 12 h at 514 nm excitation wavelength. (d) Corresponding RBM and G-band Raman spectra for batch 1 and 2 HiPco SWCNTs at 633 nm excitation wavelength similar to (a). The RBMs were normalized with respect to the G-band. M_{ii} and S_{ii} correspond to metallic and semiconducting interband transitions.

semiconducting peaks (s-peaks) remained intact without a shift of the peak position, while maintaining the same intensity ratio among them. The Breit−Wigner−Fano (BWF) line at the lower energy side of G-bands[29] was also drastically reduced, as shown in the right panel of Figure 2a, again indicating the removal of metallicity in the acid-treated samples. This phenomenon was fully reproducible with a different batch of HiPco SWCNTs. The second batch (batch 2) contained nanotubes with different diameter distributions, that is, higher metallicity at an excitation wavelength of 514 nm, as shown in the RBM (Figure 2b). The m-peaks were again mostly removed, whereas the s-peaks were significantly enlarged. Since adsorbates were fully removed by the heat treatment at 900 °C, as evidenced by the XPS data later, the removal of m-SWCNTs should be independent of the adsorbate effect. The D-band was slightly developed in this case, suggesting that the remaining SWCNTs were partially attacked during the treatment. On the other hand, the filtrated sample showed no RBM peaks and a prominently developed D-band (Figure 2c), which is characteristic of amorphous carbons. This observation is consistent with the FESEM image (Figure 1), showing that nanotubes were disintegrated into the carbonaceous particles. This can be also evidenced by the amount of loss (30−35 wt %) of the SWCNTs after the HNO_3/H_2SO_4 treatments.

The resonant Raman spectra of the pristine sample at an excitation wavelength of 633 nm showed two m-peaks near 191 and 215 cm^{-1} and two s-peaks near 255 and 281 cm^{-1} (Figure 2d). With HNO_3/H_2SO_4 (1:9) treatment of 12 h and subsequent heat treatment (batch 1), the s-peak near 281 cm^{-1} (diameter ∼ 0.88 nm) was removed, suggesting that even s-SWCNTs with smaller diameters were removed. The rest of the peaks remained with a similar intensity ratio. The slight enhancement of the BWF line in the G-band after HNO_3/H_2SO_4 treatment of 12 h reflects the reduction of s-SWCNTs (diameter ∼ 0.88 nm). With longer HNO_3/H_2SO_4 treatment of 48 h, the s-peak near 255 cm^{-1} (diameter ∼ 0.99 nm) was rather intensified compared to the pristine sample, which was accompanied by considerable decrease of the m-peak intensity near 191 cm^{-1}, resulting in slight decrease of the BWF line intensity. The m-peak (near 191 cm^{-1}) should be related to both chiral and achiral (armchair and zigzag) nanotubes.[17,30] According to the report by Menna et al., they assigned such an intensity decrease of the m-peak (near 191 cm^{-1}) to higher reactivity of metallic zigzag nanotubes toward oxidation.[17] Therefore, our result was probably associated with a lower adsorption barrier of metallic zigzag nanotubes with NO_2^+, which was also supported by our theoretical investigation of NO_2 reactivity on SWCNTs, reported elsewhere.[31] Batch 2 showed a tendency similar to that of batch 1 (Figure 2d). At 785 nm, we also observed that s-SWCNTs with diameters less than 1.1 nm in the RBM were preserved even after HNO_3/H_2SO_4 (1:9) treatments of 48 h (Figure 3). The peak intensities near 200 and 263 cm^{-1} relatively increased, compared to that near 225 cm^{-1}, which should be associated with an aggregation effect of SWCNTs after HNO_3/H_2SO_4 treatment.[32] Here, we again emphasize that m-peaks near 260 cm^{-1} at an excitation wavelength of 514 nm were completely removed. Therefore, there is a clear selectivity between m-SWCNT and s-SWCNT in the small-diameter SWCNTs (0.9−1.1 nm). As mentioned above, however, all the tubes with small diameters

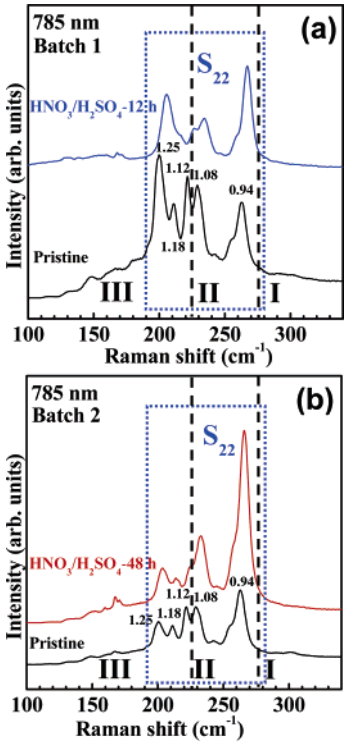

Figure 3. RBM Raman spectra from the leftover on the filter for batch 1 (a) and batch 2 (b) HiPco SWCNTs at 785 nm excitation wavelength. The black, blue, and red lines are from the pristine, HNO_3/H_2SO_4 (1:9) treatment for 12 h, and HNO_3/H_2SO_4 (1:9) treatment for 48 h, respectively, followed by heat treatment at 900 °C in Ar atmosphere. M_{ii} and S_{ii} correspond to metallic and semiconducting interband transitions.

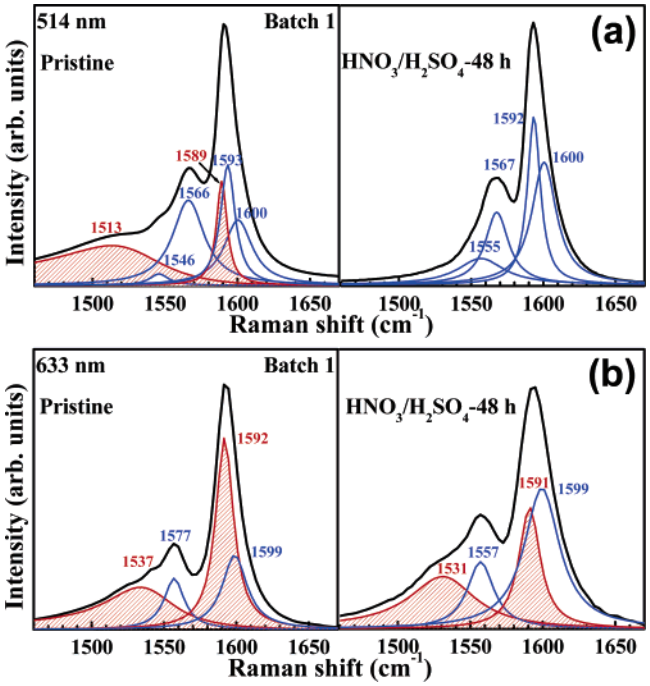

Figure 4. Fitting of G-band Raman spectra at excitation wavelengths of (a) 514 and (b) 633 nm for batch 1 HiPco SWCNTs before and after HNO_3/H_2SO_4 (1:9) treatment for 48 h, followed by heat treatment at 900 °C in Ar atmosphere. The metallic and semiconducitng peaks were fitted using BWF and Lorentzian lines. The asymmetric BWF line shape is described by $I(\omega) = I_0([1 + (\omega - \omega_{BWF})/q\Gamma]^2)/(1 + [(\omega - \omega_{BWF})/\Gamma]^2)$, where $1/q$ is a measure of the interaction of the phonon with a continuum of states and ω_{BWF} is the BWF peak frequency at maximum intensity I_0.[33]

less than 0.9 nm seemed to be etched away due to heavy strain, independent of metallicity (Figure 2a,b,d). Moreover, the large-diameter m-SWCNTs near 191 cm^{-1} were reduced significantly but the m-peak at 215 cm^{-1} was still present in the sample even after the HNO_3/H_2SO_4 treatment of 48 h, as shown in Figure 2d. Thus, the selective removal of m-SWCNTs becomes obscured at diameters greater than 1.1 nm. The similar behavior of the diameter-selective removal of m-SWCNTs was also obtained in batch 2 (Figures 2b,d and 3b).

We separated the RBM into three regions in order to explain the diameter dependence in a selective attack of SWCNTs by HNO_3/H_2SO_4 treatment, as indicated in Figures 2 and 3. In regime I, where the diameters are less than 0.9 nm, all SWCNTs were etched away. In regime II, where the diameters range from 0.9 to 1.1 nm, s-SWCNTs remained intact, whereas all m-SWCNTs were etched away. In regime III, where the diameters are greater than 1.1 nm, the m-SWCNTs were reduced significantly but not completely. If one uses starting SWCNTs with diameters less than 1.1 nm, only s-SWCNTs could be obtained on a large scale.

We provide a detailed analysis of the G-band in Figure 4. The pristine sample at 514 nm (Figure 4a) had two metallic (m) components (red) with a BWF line near 1513 cm^{-1} and a Lorentzian line near 1589 cm^{-1}, and four semiconducting (s) components (blue) with Lorentzian lines near 1546, 1566, 1593, and 1600 cm^{-1}, similar to the previous report.[33] Two m-components were completely removed after HNO_3/H_2SO_4 treatment, while s-components were intensified without a significant change in the peak positions. At 633 nm (Figure 4b), the pristine sample was fitted using two m-components and two s-components. After HNO_3/H_2SO_4 (1:9) treatment, the intensities of m-components were reduced, whereas those of s-components were enlarged. Therefore, these results again demonstrated the removal of small-diameter m-SWCNTs (at 514 nm) and the reduction of large-diameter m-SWCNTs (at 633 nm) in the HNO_3/H_2SO_4-treated sample.

To confirm the dependence of HNO_3/H_2SO_4 volume ratios in the diameter-selective removal of m-SWCNTs, we analyzed the RBM Raman spectra (514 and 633 nm) of SWCNTs treated with various volume ratios (1:9, 1:3, and 1:2) for 12 h (Figure 5). The RBM Raman spectra of SWCNTs treated with HNO_3/H_2SO_4 volume ratios of 1:3 and 1:2 show a tendency similar to that of the 1:9 sample. With HNO_3/H_2SO_4 treatments, m-SWCNTs are completely removed for SWCNTs with small diameters less than 1.1 nm (Figure 5a), while s-SWCNTs less than 1.1 nm remain intact (Figure 5b), regardless of HNO_3/H_2SO_4 volume ratios.

We also analyzed the RBM in Raman spectra (514, 633, and 785 nm) of the air-oxidized SWCNTs, which were heated in an air flow (350 °C, 1 h) without any further treatment (Figure S1 in the Supporting Information), to elucidate the difference in reactivity of SWCNTs between HNO_3/H_2SO_4 and simple gas-phase oxidation. After the gas-phase oxidation, the RBM peak intensities of SWCNTs with small diameters were dramatically reduced, regardless of metallicity. It is interesting to note that the gas-phase oxidation treatment clearly led to the diameter-selective removal of SWCNTs, which is in good agreement with previous studies,[13,14] whereas the HNO_3/H_2SO_4 treatment strongly depended on the metallicity of SWCNTs.

Although Raman spectra provided some information for the removal of m-SWCNTs, this was excitation energy dependent due to the nature of the resonant Raman behavior and therefore could not provide quantitative information for the metallicity of SWCNTs with the limited number of excitation sources. Here

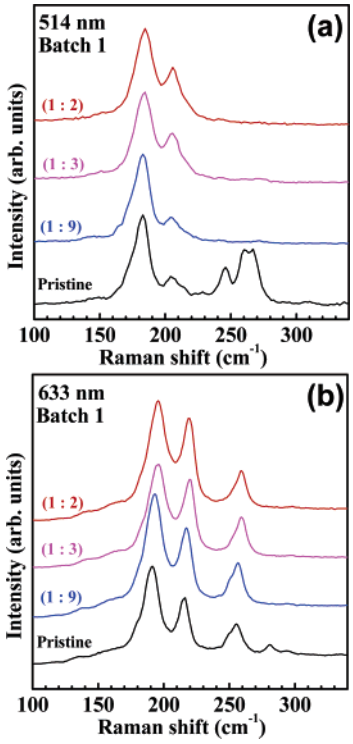

Figure 5. RBM Raman spectra at excitation wavelengths of (a) 514 and (b) 633 nm from the leftover on the filter for batch 1 HiPco SWCNTs treated with HNO_3/H_2SO_4 solutions of different volume ratios for 12 h, followed by heat treatment at 900 °C in Ar atmosphere. HNO_3 and H_2SO_4 were mixed in three different volume ratios of 1:9, 1:3, and 1:2, respectively.

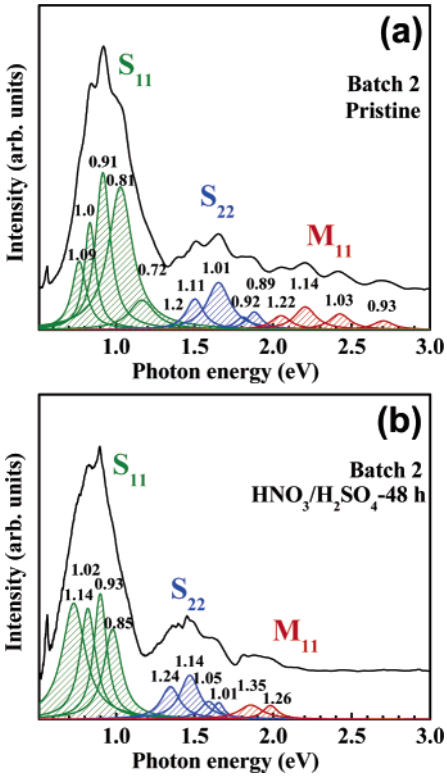

Figure 6. Subtraction of baselines and Lorentzian fittings for optical absorption spectra for batch 2 HiPco SWCNTs. Absorption spectra from (a) the pristine and (b) HNO_3/H_2SO_4 (1:9) treated samples for 48 h, followed by heat treatment at 900 °C in Ar atmosphere. M_{ii} and S_{ii} correspond to metallic and semiconducting interband transitions.

we provide optical absorption spectra to determine the overall content of m-SWCNTs. The spectrum was composed of three bands, two semiconducting S_{11} and S_{22} and one metallic M_{11} interband transitions (Figure 6).[34] Each subband peak is closely related to the SWCNT diameter. The diameter ranges (0.7−1.2 nm for semiconducting and 0.9−1.3 nm for metallic nanotubes) determined from the tight-binding model were in good agreement with that obtained from the Raman spectra (the agreement is better with the modified relationship between the transition energy and diameter that is based on trigonal warping effect).[34] We emphasize that m-SWCNTs with small diameters less than 1.1 nm were removed, whereas s-SWCNTs with small diameters of up to 0.85 nm were still retained in the sample. These changes were in excellent agreement with observations from Raman spectra. Since the S_{11} band might be modified more easily than the S_{22} band,[34,36] we extracted information for the content of m-SWCNTs using S_{22} by $M_{11}/(M_{11} + S_{22})$. This value was 38% from the pristine sample, comparable to the theoretically estimated value of 30%. The content of m-SWCNTs in the acid-treated sample was significantly reduced to 20% due to removal of m-SWCNTs with small diameters.

The selective removal of m-SWCNTs can be understood by NO_2^+ adsorption on nanotubes. O 1s XPS spectra show that the C−O bonds near 532.3 eV are developed with HNO_3/H_2SO_4 (1:9) treatment[37] and reversed after heat treatment at 900 °C (Figure 7a). This is in somewhat good contrast to the general belief that N sites in NO_2^+ prefer to adsorb on the nanotube surface, not O sites. N 1s XPS spectra also show that the amount of C−N related peaks is increased with HNO_3/H_2SO_4 (1:9) treatment of 48 h (Figure 7a). The adsorption of NO_2^+ involves strong charge transfer between nanotubes and nitronium ions, thus shifting the peak positions in the Raman spectra; the peak positions were recovered after heat treatment, indicating recovery of electronic structures of nanotubes (Figure S2 in the Supporting Information). Moreover, the disappeared m-peaks (514 nm) by HNO_3/H_2SO_4 treatment were still not visible even after post heat treatment (Figure S2), which is in good contrast to the diazonium treatment reported previously.[11] This N 1s peak again disappeared after heat treatment. This implies that the NO_2^+ can be adsorbed at first on the nanotube wall in various forms and desorbed in the following heat treatment. The adsorption of NO_2^+ is promoted by the presence of H_2SO_4 that can be easily intercalated into the SWCNT bundles in the form of H_2SO_4. This priori intercalation process is necessary to provide more available surface for NO_2^+ to adsorb on the tube wall. Once NO_2^+, particularly oxygen sites, is adsorbed on the tube wall, the tube walls can easily be damaged and disintegrated, similar to etching processes under oxygen gas atmosphere.

To understand the adsorption energetics of the NO_2^+, we performed first-principles calculations for NO_2 adsorption on (n,0) zigzag nanotubes using GGA.[19] The nanotube can be regarded as a metallic (or semimetallic) one, when n is a multiple of 3. Otherwise they are semiconducting with a finite band gap. Figure 7b shows a physisorbed NO_2 molecule on the nanotube wall. The computed adsorption energies (E_{ad}) for various sizes of nanotubes are given in Table 1. We note that E_{ad} on m-SWCNTs was consistently lower than that on s-SWCNTs. The difference became smaller with increasing diameters, which is a consequence of smaller energy gaps for s-SWCNTs with larger diameters. From the analysis on the electron densities (Figure S3 in the Supporting Information), we found that the amount of charge transfer from the nanotube to NO_2 molecule was enhanced for m-SWCNTs. This will be even bigger for positively charged NO_2^+ used in real experiments. On the other hand, we also calculated precursor states, where one of the

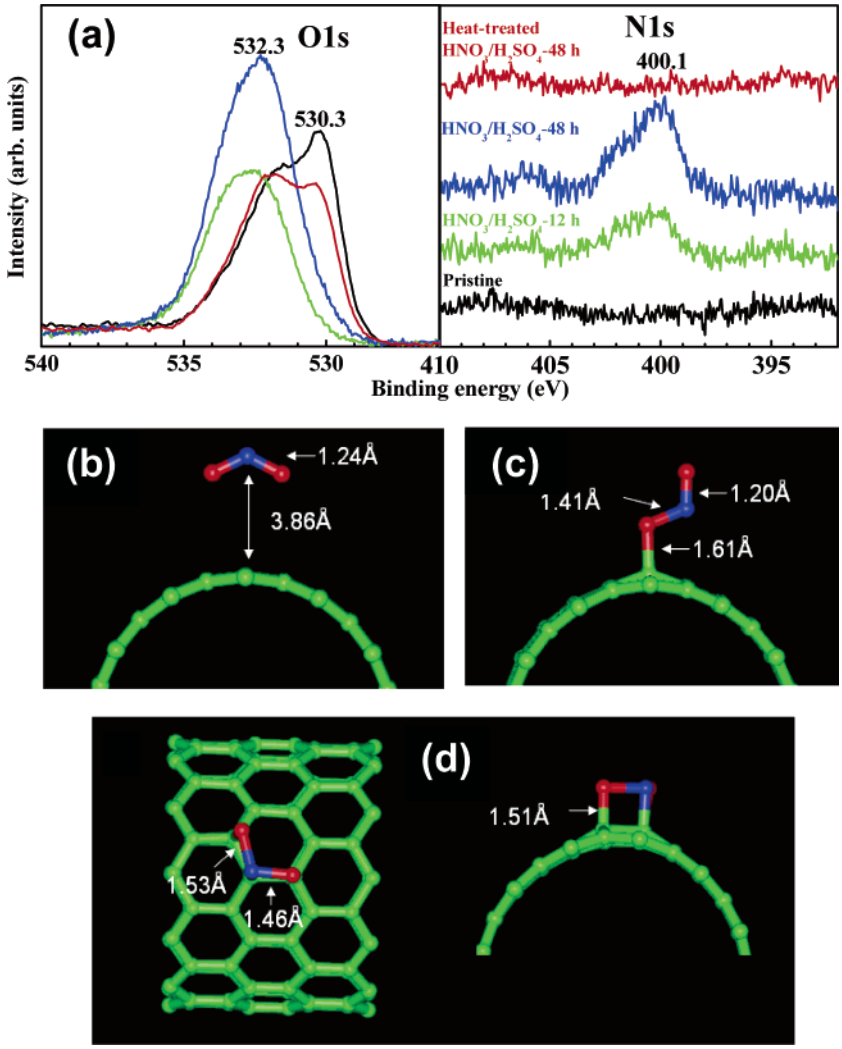

Figure 7. (a) XPS spectra of O 1s and N 1s for batch 1 HiPco SWCNTs. The pristine sample (black), HNO_3/H_2SO_4 (1:9) treated ones for 12 h (green), and HNO_3/H_2SO_4 (1:9) treated ones for 48 h (blue), followed by heat treatment at 900 °C in Ar atmosphere (red). (b), (c), and (d) are the geometric models for physisorbed and precursor states on the (12,0) nanotube, which were determined from the density functional calculations. The red and blue atoms indicate oxygen and nitrogen atoms, respectively.

TABLE 1: Adsorption Energies Calculated from GGA for Various Diameters of Nanotubes

(*n*,0)	(9,0)	(10,0)	(11,0)	(12,0)	(17,0)	(18,0)
diameter (nm)	0.71	0.79	0.87	0.95	1.33	1.42
E_{ad} (eV)						
physisorbed (Figure 7b)	−0.39	−0.28	−0.26	−0.37	−0.29	−0.34
precursor (Figure 7c)	0.12	0.40	0.46	0.36	unstable	unstable
precursor (Figure 7d)	2.02	2.43	2.52	2.60	3.11	3.08

oxygen atoms was chemically bound to the tube wall (Figure 7c) or an NO_2 molecule was attached parallel to the surface (Figure 7d). These are possible intermediate states along the path to the disintegration of nanotubes. The latter configuration involves both C−O and C−N chemical bonds, in excellent agreement with the XPS data among model systems considered here. The energy loss compared to the physisorbed configuration was attributed to the deformation of the nanotube and the NO_2 molecule. The adsorption could become exothermic in the bundled nanotubes in liquid state or by cooperative processes involving several molecules.[38] The exothermic adsorption energetics could be also realized by an additional adsorption of hydroxyl group. The tendency of E_{ad} for precursor states shown in Table 1 indicates that the curvature of the nanotube wall plays an important role in stabilizing precursor states, especially in the case of precursor (Figure 7d), where E_{ad} monotonically increases with the nanotube radius. These precursor states could be transformed to strongly chemisorbed ones by being squeezed into the bundles. Therefore, the selectivity addressed by the physisorbed configuration will result in the removal of the metallic component efficiently for small-diameter nanotubes. The theoretically predicted energetics of NO_2 adsorption may not be directly applicable to the experiments that were done in a liquid phase. Moreover, the adsorption energy could be enhanced by the presence of the SWCNT bundles. Nevertheless, it should be stressed that this theoretical prediction is consistent with the above experimental observations that the selective removal is most clear for nanotubes with diameters less than 1.1 nm.

Conclusions

We have clearly presented that m-SWCNTs with small diameters less than 1.1 nm are selectively removed by using

HNO_3/H_2SO_4 treatment. The selective etching of small-diameter m-SWCNTs should be achieved by an attack of NO_2^+ during the HNO_3/H_2SO_4 treatment, which was supported by our previous report on NHFA treatment of SWCNTs.[18] The selective removal of small-diameter m-SWCNTs by HNO_3/H_2SO_4 treatment was more effective compared with that by the NHFA treatment.[18] Positively charged NO_2^+ preferred to selectively adsorb on m-SWCNTs with stronger binding energy compared to the counterpart s-SWCNTs. This was attributed to more available electron densities at the Fermi level in m-SWCNTs. This difference became obscured for SWCNTs with diameters greater than 1.1 nm. This strain-induced chirality separation by NO_2^+ was confirmed by our theoretical calculations. The small-diameter m-SWCNTs strongly bound with NO_2^+ by HNO_3/H_2SO_4 treatment were destroyed and the Raman peak positions of the remaining s-SWCNTs were recovered by thermal annealing at high temperature, suggesting that the electronic structures of nanotubes are almost recovered after post heat treatment. We expect that our approach of the mild acid treatment followed by thermal annealing could provide a novel route to separate s-SWCNTs from a mixture of m- and s-SWCNTs in mass quantity, although the chirality selectivity was not clear for SWCNTs with diameters greater than 1.1 nm. The selectivity relies strongly on the nanotube diameter, and a more sophisticated process should be designed for a higher yield of s-SWCNTs. We again emphasize that the selective removal of small-diameter m-SWCNTs by NO_2^+ produced from HNO_3/H_2SO_4 solution presented a striking contrast to the diameter-selective removal of SWCNTs by oxidative treatments reported previously.[13−16]

Acknowledgment. This research was supported by a grant (05K1401-00412) from Center for Nanoscale Mechatronics & Manufacturing and TND project, one of the 21st Century Frontier Research Programs, which are supported by Ministry of Science and Technology in Korea, and CNNC at SKKU.

Supporting Information Available: Figure S1, RBM Raman spectra (514, 633, and 785 nm) for air-oxidized HiPco SWCNTs; Figure S2, RBM Raman spectra (514 nm) for HNO_3/H_2SO_4 (1:9) treated HiPco SWCNTs before and after heat treatment at 900 °C; Figure S3, redistribution of electronic density as calculated by $\Delta\rho = \rho(\mathrm{CNT}+\mathrm{NO_2}) - \rho(\mathrm{CNT}) - \rho(\mathrm{NO_2})$. This material is available free of charge via the Internet at http://pubs.acs.org.

References and Notes

(1) Tans, S. J.; Verschueren, A. R. M.; Dekker, C. *Nature* **1998**, *393*, 49.

(2) An, K. H.; Kim, W. S.; Park, Y. C.; Bae, D. J.; Choi, Y. C.; Lee, S. M.; Chung, D. C.; Lim, S. C.; Lee, Y. H. *Adv. Mater.* **2001**, *13*, 497.

(3) Iijima, S.; Ichihashi, T. *Nature (London)* **1993**, *363*, 603.

(4) Bethune, D. S.; Kiang, C. H.; de Vries, M. S.; Gorman, G.; Savoy, R.; Vazquez, J.; Beyers, R. *Nature (London)* **1993**, *363*, 605.

(5) Thess, A.; Lee, R.; Nikolaev, P.; Dai, H.; Petit, P.; Robert, J.; Xu, C.; Lee, Y. H.; Kim, S. G.; Rinzler, A. G.; Colbert, D. T.; Scuseria, G. E.; Tomanek, D.; Fischer, J. E.; Smalley, R. E. *Science* **1996**, *273*, 483.

(6) Krupke, R.; Hennrich, F.; Lohneysen, H. V.; Krappes, M. M. *Science* **2003**, *301*, 344.

(7) Zheng, M.; Jagota, A.; Semke, E. D.; Diner, B. A.; Mclean, R. S.; Lustig, S. R.; Richardson, R. E.; Tass, N. G. *Nat. Mater.* **2003**, *2*, 338.

(8) Zheng, M.; Jagota, A.; Strano, M. S.; Santos, A. P.; Barone, P.; Chou, S. G.; Diner, B. A.; Dresselhaus, M. S.; Mclean, R. S.; Onoa, G. B.; Samsonidze, G. G.; Semke, E. D.; Usrey, M.; Walls, D. J. *Science* **2003**, *302*, 1545.

(9) Chattopadhyay, D.; Galeska, I.; Papadimitrakopoulos, F. *J. Am. Chem. Soc.* **2003**, *125*, 3370.

(10) Chen, Z.; Du, X.; Du, M.-H.; Daniel Rancken, C.; Cheng, H.-P.; Rinzler, A. G. *Nano Lett.* **2003**, *3*, 1245.

(11) Strano, M. S.; Dyke, C. A.; Usrey, M. L.; Barone, P. W.; Allen, M. J.; Shan, H.; Kittrell, C.; Hauge, R. H.; Tour, J. M.; Smalley, R. E. *Science* **2003**, *301*, 1519.

(12) Banerjee, S.; Wong, S. S. *J. Am. Chem. Soc.* **2004**, *126*, 2073.

(13) Zhou, W.; Ooi, Y. H.; Russo, R.; Papanek, P.; Luzzi, D. E.; Fischer, J. E.; Bronikowski, M. J.; Willis, P. A.; Smalley, R. E. *Chem. Phys. Lett.* **2001**, *350*, 6.

(14) Wiltshire, J. G.; Khlobystov, A. N.; Li, L. J.; Lyapin, S. G.; Briggs, G. A. D.; Nicholas, R. J. *Chem. Phys. Lett.* **2004**, *386*, 239.

(15) Banerjee, S.; Wong, S. S. *Nano Lett.* **2004**, *4*, 1445.

(16) Yudasaka, M.; Zhang, M.; Iijima, S. *Chem. Phys. Lett.* **2003**, *374*, 132.

(17) Menna, E.; Negra, F. D.; Fontana, M. D. *Phys. Rev. B* **2003**, *68*, 193412.

(18) An, K. H.; Park, J. S.; Yang, C.-M.; Jeong, S. Y.; Lim, S. C.; Kang, C.; Son, J.-H.; Jeong, M. S.; Lee, Y. H. *J. Am. Chem. Soc.* **2005**, *127*, 5196.

(19) Perdew, J. P.; Burke, K.; Ernzerhof, M. *Phys. Rev. Lett.* **1996**, *77*, 3865.

(20) Baroni, S.; Dal Corso, A.; de Gironcoli, S.; Giannozzi, P. http://www.pwscf.org.

(21) Vanderbilt, D. *Phys. Rev. B* **1990**, *41*, 7892.

(22) Moon, J.-M.; Park, Y. S.; An, K. H.; Park, G.-S.; Lee, Y. H. *J. Phys. Chem. B* **2001**, *105*, 5677.

(23) Wiltshire, J. G.; Khlobystov, A. N.; Li, L. J.; Lyapin, S. G.; Briggs, G. A. D.; Nicholas, R. J. *Chem. Phys. Lett.* **2004**, *386*, 239.

(24) Liu, J.; Rinzler, A. G.; Dai, H.; Hafner, J. H.; Bradley, R. K.; Boul, P. J.; Lu, A.; Iverson, T.; Shelimov, K.; Huffman, C. B.; Rodriguez-Macias, F.; Shon, Y.-S.; Lee, T. R.; Colbert, D. T.; Smalley, R. E. *Science* **1998**, *280*, 1253.

(25) Peng, H.; Alemany, L. B.; Margrave, J. L.; Khabashesku, V. N. *J. Am. Chem. Soc.* **2003**, *125*, 15174.

(26) Carey, F. A. *Organic Chemistry*; McGraw-Hill: New York, 1996.

(27) Kramberger, Ch.; Pfeiffer, R.; Kuzmany, H.; Zolyomi, V.; Kurti, J. *Phys. Rev. B* **2003**, *68*, 235404.

(28) Kataura, H.; Kumazawa, Y.; Maniwa, Y.; Umezu, I.; Suzuki, S.; Ohtsuka, Y.; Achiba. Y. *Synth. Met.* **1999**, *103*, 2555.

(29) Eklund, P. C.; Subbaswamy, K. R. *Phys. Rev. B* **1979**, *20*, 5157.

(30) Fantini, C.; Jorio, A.; Souza, M.; Strano, M. S.; Dresselhaus, M. S.; Pimenta, M. A. *Phys. Rev. Lett.* **2004**, *93*, 147406.

(31) Seo, K.; Park, K. A.; Kim, C.; Han, S.; Kim, B.; Lee, Y. H. Submitted for publication in *J. Am. Chem. Soc.* **2005**.

(32) Heller, D. A.; Barone, P. W.; Swanson, J. P.; Mayrhofer, R. M.; Strano, M. S. *J. Phys. Chem. B* **2004**, *108*, 6905.

(33) Brown, S. D. M.; Jorio, A.; Corio, P.; Dresselhaus, M. S.; Dresselhaus, G.; Saito, R.; Kneipp, K. *Phys. Rev. B* **2001**, *63*, 155414.

(34) Itkis, M. E.; Perea, D. E.; Niyogi, S.; Rickard, S. M.; Hamon, M. A.; Hu, H.; Zhao, B.; Haddon, R. C. *Nano Lett.* **2003**, *3*, 309.

(35) Liu, X.; Pichler, T.; Knupfer, M.; Golden, M. S.; Fink, J.; Kataura, H.; Achiba, Y. *Phys. Rev. B* **2002**, *66*, 045411.

(36) Chen, J.; Hamon, M. A.; Hu, H.; Chen, Y.; Rao, A. M.; Eklund, P. C.; Haddon, R. C. *Science* **1998**, *282*, 95.

(37) Pels, J. R.; Kapteijn, F.; Moulijn, J. A.; Zhu, Q.; Thomas, K. M. *Carbon* **1995**, *33*, 1641.

(38) Yim, W.-L.; Gong, X. G.; Liu, Z.-F. *J. Phys. Chem. B* **2003**, *107*, 9363.